Surface & Coatings Technology 382 (2020) 125154

Contents lists available at ScienceDirect

Surface & Coatings Technology

journal homepage: www.elsevier.com/locate/surfcoat

Photocatalytic activity of TiO_2 films prepared by cathodic arc deposition: Dependence on thickness and reuse of the photocatalysts

A. Kleiman[a,b,*], J.M. Meichtry[c,d], D. Vega[e,f], M.I. Litter[c,g], A. Márquez[a,b]

[a] Universidad de Buenos Aires, Facultad de Ciencias Exactas y Naturales, Departamento de Física, Buenos Aires, Argentina
[b] Universidad de Buenos Aires, Consejo Nacional de Investigaciones Científicas y Técnicas, Instituto de Física del Plasma (INFIP), Facultad de Ciencias Exactas y Naturales, Ciudad Universitaria Pab. I, 1428 Buenos Aires, Argentina
[c] Gerencia Química, Comisión Nacional de Energía Atómica-CONICET, Av. Gral. Paz 1499, 1650 San Martín, Prov. de Buenos Aires, Argentina
[d] Universidad Tecnológica Nacional, Facultad Regional Buenos Aires, Departamento de Ingeniería Química, Medrano 951, C1179 Buenos Aires, Argentina
[e] Departamento Física de la Materia Condensada, Gerencia de Investigación y Aplicaciones, Comisión Nacional de Energía Atómica, Av. Gral. Paz 1499, 1650 San Martín, Prov. de Buenos Aires, Argentina
[f] Escuela de Ciencia y Tecnología, Universidad Nacional de San Martín, Provincia de Buenos Aires, Argentina
[g] IIIA-Instituto de Investigación e Ingeniería Ambiental, Universidad Nacional de General San Martín-CONICET, Campus Miguelete, Av. 25 de Mayo y Francia, 1650 San Martín, Prov. de Buenos Aires, Argentina

ARTICLE INFO

Keywords:
Titanium dioxide
Thin films
Cathodic arcs
Heterogeneous photocatalysis
Cr(VI) photocatalytic reduction
Photocatalyst reuse

ABSTRACT

In this work, the photocatalytic activity of anatase films with thicknesses up to 1100 nm prepared by cathodic arc deposition (CAD) on glass substrates is reported. The photocatalytic activity under UV–Vis irradiation ($\lambda > 330$ nm) was evaluated through the efficiency in the reduction of 0.80 mM Cr(VI) in the presence of 1 mM ethylenediaminetetraacetic acid (EDTA) at pH 2, and compared with the performance of samples obtained by dip-coating using commercial P25. The CAD films were optically transparent, with visible light transmittance ≥ 50% even for the thickest samples. The photocatalytic efficiency of the films increased as the thickness increased. The possibility of obtaining thicker films allowed cathodic arc films reaching better performance than P25 samples. For the most active films obtained by CAD, complete Cr(VI) reduction could be obtained in < 300 min under a 28 W m^{-2} UV-A irradiance. The photocatalytic reaction for all the studied TiO_2 films obeyed pseudo-first order kinetics. A decrease of the reaction rate constant was observed for both types of films after reusing the photocatalysts. The fate of the reduced Cr(VI) was also analyzed.

1. Introduction

Among many other applications, titanium dioxide has been widely investigated as a photocatalyst for degradation of pollutants in water and self-cleaning surfaces. The photocatalytic activity of TiO_2 takes place under UV irradiation, given the band gap of the semiconductor (~3.2 eV for anatase) [1,2]; among the different TiO_2 crystalline structures, anatase (A) is considered the most photocatalytically active phase [3]. Commercially available AEROXIDE® TiO_2 P 25 (Evonik), P25 from now on, composed of mainly A (70–80%) and a small amount of rutile (R) (20–30%) ([4] and references therein), presents outstanding photocatalytic efficiency, and it has been established as a reference material [4,5]. Investigations in this field have initially focused on the study of the photocatalytic activity of TiO_2 particles in aqueous suspensions, later turning to supported TiO_2 to avoid the final separation process of the photocatalyst in the application; besides, immobilized TiO_2, either as powder or as thin films, has also attracted much attention due to its possible application in gas phase photocatalysis and for preparation of self-cleaning and/or superhydrophilic surfaces [1,6,7].

The study of the photocatalytic activity of TiO_2 films under UV irradiation remains an active field of research; in particular, many works have been published in recent times focusing on the use of pure and doped TiO_2 films for the photocatalytic reduction of Cr(VI) (e.g. [8–17]), a toxic and carcinogenic pollutant present in wastewaters from different industries, although it can also be found naturally and/or coming from agricultural activities [18]. The Cr(VI)/ethylenediaminetetraacetic acid (EDTA) system has been found an excellent model system to test TiO_2 photocatalysts [14,19–21]. Different kinetics have been proposed and reported for the photocatalytic Cr(VI) reduction using immobilized TiO_2, i.e., zero [8,17,22], first [9,16,23–25], and half order kinetics [22,26]. In previous works, where Cr(VI) in the presence of EDTA was used as the model pollutant system, a kinetic

* Corresponding author at: Universidad de Buenos Aires, Facultad de Ciencias Exactas y Naturales, Departamento de Física, Buenos Aires, Argentina.
E-mail address: kleiman@tinfip.lfp.uba.ar (A. Kleiman).

https://doi.org/10.1016/j.surfcoat.2019.125154
Received 20 August 2019; Received in revised form 8 November 2019; Accepted 9 November 2019
Available online 12 November 2019
0257-8972/

expression composed of a first order term (which considers the photochemical homogeneous reaction Cr(VI) with EDTA) plus a zero order term (describing the heterogeneous reaction on the catalyst surface) was proposed [11,15,16]. However, a clear dependence of the kinetics on the properties of the films (i.e., TiO_2 synthesis method or film thickness) has not been reported. On the other hand, the deactivation and/or the reuse of immobilized TiO_2 after Cr(VI) photocatalytic reduction have only recently been studied by Marinho et al. [23–25], despite being extensively studied for suspended TiO_2 ([4,14,19,21,27,28] and refs. therein).

Several techniques have been attempted for the formation of TiO_2 films, such as chemical vapor deposition (CVD), physical vapor deposition (PVD), electrodeposition, electrophoresis, laser ablation, plasma spray, sputtering, anodization, thermal oxidation of metallic Ti, sol-gel, impregnation from nanoparticle suspensions, etc., all of them presenting limitations or high costs [15]. On the other hand, cathodic arc deposition (CAD) has demonstrated to be a suitable method, enabling the control of the TiO_2 crystalline phases, together with other optical and mechanical properties, at rather low temperatures [29–31]. Besides, CAD films present excellent adhesion to the substrate, especially when compared with films obtained from TiO_2 suspensions [15,23]. Despite the extensive literature on TiO_2 films prepared by CAD, studies on the photocatalytic activity have been scarcely reported, mainly addressing the degradation of dyes [32,33], and one preliminary work on bacterial inactivation [34]. Regarding Cr(VI) reduction, only our previous study on TiO_2 films grown by CAD has been reported [15]. In that work, CAD films with thickness up to 700 nm showed good photocatalytic activity but somewhat lower than P25 films.

In this work, the study of the photocatalytic activity of TiO_2 films deposited by CAD on glass substrates was extended to thicknesses up to 1100 nm in order to enhance the photocatalytic efficiency. The photocatalytic activity was evaluated through the efficiency in the reduction of Cr(VI) in the presence of EDTA. The response of these coatings was compared with the performance of films obtained by dip-coating using commercial P25. The reaction kinetics, the fate of the reduced Cr(VI) and the efficiency when reusing the films were analyzed.

2. Experimental section

2.1. Chemicals and materials

Potassium dichromate was from Merck (99.9%), EDTA (99%) was from Riedel de Häen, phosphoric acid (H_3PO_4, 85%) was from Biopack, diphenylcarbazide (DPC) was from UCB for analysis, and acetone was from Merck (99.5%). Diluted perchloric acid (70%, Biopack) was used for pH adjustments. All other reagents were of analytical grade and used as received. All solutions and suspensions were prepared with Milli-Q grade water (resistivity = 18 MΩ cm), Osmoion Apema. When filtration was needed, Millipore acetate cellulose filters (25 mm diameter, 0.22 μm pore size) were used.

2.2. Film grow method

Optically transparent TiO_2 films were grown by CAD. The employed vacuum arc system comprised a cylindrical stainless steel chamber (25 cm diameter, 50 cm length) which acted as anode. The cathode (Ti grade 2, 55 mm diameter) was placed coaxially at one end of the chamber; at the other end the substrate holder was held. A detailed description of the device can be found in previous works [35]. Depositions were carried out with an arc current of 100 A in an O_2 atmosphere at a pressure of 3 Pa. Square pieces (2.5 cm × 2.5 cm) of borosilicate glass were used as substrates, which were placed facing the cathode at 26 cm from its surface. Films were grown at room temperature and later annealed at 400 °C during 1 h in air at atmospheric pressure. Deposition time was varied in order to obtain different film thickness; samples with film thickness of 200 ± 50, 400 ± 80, 750 ± 90, 900 ± 100, 1000 ± 120 and 1100 ± 130 nm (CAD 200, CAD 400, CAD 750, CAD 900, CAD 1000 and CAD 1100, respectively) were synthesized.

P25 films were also prepared as described previously [15]. Briefly, the films were prepared by dip-coating on a borosilicate glass substrate, identical to that used for the CAD films, in a P25 suspension (Evonik), 5% (*w/v*) at pH 2.5 in deionized water. The glass substrates were immersed in the suspension and then withdrawn at a constant speed of 3.3 mm/s. The number of immersions was varied to reach different thicknesses. After the deposition, the coating on one of the faces of the glass was quickly removed. Samples were dried in a stove at 75 °C for 20 h after each immersion, and after the last coating they were also heated at 400 °C during 1 h. P25 samples with > 10 immersions exhibited poor adhesion, and TiO_2 partially detached when put in contact with water. Samples with film thickness of 100 ± 10, 170 ± 10, 280 ± 20 and 480 ± 30 nm (P25 100, P25 170, P25 280 and P25 480, respectively) were obtained after 1, 3, 6 and 10 applications, respectively.

2.3. Characterization of the films

The mass of TiO_2 in the films was determined by weighting the glass before and after deposition treatment, including the heating at 400 °C for the P25 samples. Control experiments showed no weight differences in the glass substrate when submitted to the same thermal treatments.

Transmission of CAD films in the UV–visible range (300–800 nm) was measured with a UV-1800 Shimadzu spectrophotometer. An uncoated substrate was placed in the reference cell in order to obtain a direct measurement of the film transmittance. For P25 films, transmittance was measured in a Hewlett-Packard diode array UV–visible spectrophotometer, model HP 8453.

The crystalline structure of CAD films was identified by X-ray diffraction (XRD) in Bragg-Brentano geometry, using a Panalytical Empyrean diffractometer with a CuK_α source with a PixCel 3D detector. As previously reported [15], the XRD patterns of P25 films are identical to the pattern of P25 powder. The surface morphology was analyzed by Scanning electron microscopy (SEM) (FEG-SEM Zeiss Leo 982 GEMINI).

2.4. Cr(VI) photocatalytic reduction

An aqueous solution containing 0.8 mM Cr(VI) and 1 mM EDTA at pH 2, daily prepared, was used in the photocatalytic experiments. The photocatalyst films (2.5 cm × 2.5 cm) were immersed into 10 mL of this solution, and irradiated with a Phillips HPA 400S UV lamp (λ_{max} = 365 nm, see Fig. S1, in the supplementary material file) filtered through a borosilicate glass (λ > 330 nm, see Fig. S1) containing a 1 cm path length of Milli-Q water as IR filter; the mean UV irradiance (*E*) was 28 W m^{-2}, measured with a Spectroline model DM-365 XA radiometer. Each system was irradiated for 5 h under continuous magnetic stirring.

Samples (0.05 mL) were taken periodically and diluted 1/10 before measurement; for Cr(III)-EDTA measurements, undiluted solution spectra were taken at the end of the experiments. In the experiments with suspended TiO_2, samples were filtered before Cr(VI) and Cr(III)-EDTA measurement. All experiments were performed at least by duplicate, and the relative standard deviation between duplicates was always below 12%.

To evaluate the reuse of the films, the experiments were repeated up to four times; the films were washed with Milli-Q water after each experiment to remove unreacted Cr(VI) and EDTA.

2.5. Analytical determinations

Changes in Cr(VI) concentration were monitored by the spectrophotometric diphenylcarbazide method at 540 nm [36]; when it could

Table 1
Film thickness, TiO_2 mass per surface unit and crystalline phases of the synthesized films.

Sample	Film thickness (nm)	TiO_2 mass per surface unit (mg cm^{-2})	Crystalline phase A: anatase, R: rutile
CAD 200	200 ± 50	0.077 ± 0.015	A
CAD 400	400 ± 80	0.153 ± 0.018	A
CAD 750	750 ± 90	0.288 ± 0.013	A
CAD 900	900 ± 100	0.341 ± 0.014	A
CAD 1000	1000 ± 120	0.395 ± 0.016	A (93%), R (7%)
CAD 1100	1100 ± 130	0.443 ± 0.017	A (86%), R (14%)
P25 100	100 ± 10	0.030 ± 0.003	A (80%), R (20%)
P25 170	170 ± 10	0.048 ± 0.004	A (80%), R (20%)
P25 280	280 ± 20	0.080 ± 0.005	A (80%), R (20%)
P25 480	480 ± 30	0.139 ± 0.007	A (80%), R (20%)

not be detected by this method, Cr(VI) removal was considered complete. The concentration of Cr(III)–EDTA in solution was measured at 540 nm (ε = 14 m^2 mol^{-1} [37]), where neither free Cr(III) [38,39] nor Cr(VI) species [40,41] interfere. Other possible complexes of Cr(III) with EDTA photocatalytic degradation byproducts can be neglected, as established in previous works [4,27]. Cr(VI) measurements were performed in a Hewlett-Packard diode array UV–visible spectrophotometer, model HP 8453.

3. Results and discussion

3.1. Characterization of the films

The thickness of the films was estimated from the deposited mass considering the film density obtained in a previous work ((2.9 ± 0.1) g cm^{-3} for the P25 films [15], (3.85 ± 0.25) g cm^{-3} for the CAD films, average value of densities of CAD films obtained under similar conditions [15,42]). The film thickness, TiO_2 mass per cm^2 and the crystalline phase of each film, determined from XRD analysis (see below), are indicated in Table 1.

XRD diffractograms corresponding to the thinnest (200 nm) and the thickest (1100 nm) TiO_2 films prepared by CAD are shown in Fig. 1, where anatase and rutile Bragg peak positions are indicated with black and blue lines, respectively. For CAD 200 only peaks associated to the A phase were noticeable. The pattern corresponding to CAD 1100 exhibited more intense A peaks, due to greater TiO_2 mass, and also small peaks associated to R phase could be noticed. The inset in Fig. 1 shows XRD signals obtained from all the CAD films in the range corresponding to the main A and R peaks (diffraction angle 2θ between 22° and 30°). Rutile content, which was observed only in the thickest CAD films (CAD 1000 and CAD 1100), was estimated using Eq. (1) [43]:

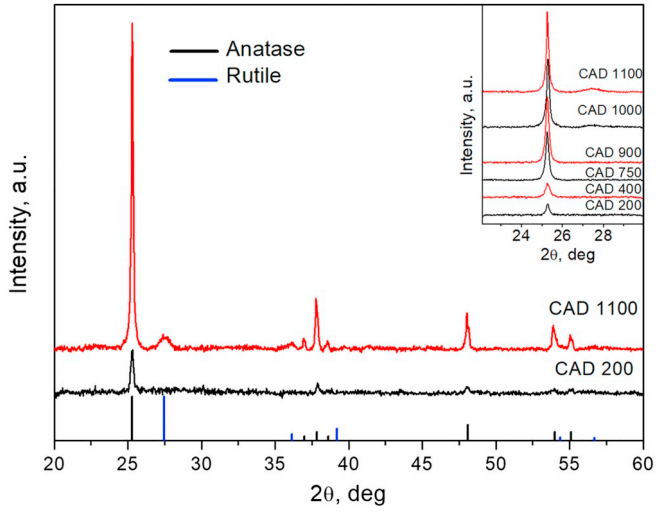

Fig. 1. XRD patterns of the CAD 200 and CAD 1100 TiO_2 films. Bragg peak positions corresponding to A and R are shown as black and blue lines, respectively. The inset figure shows diffractograms from all the CAD films in the region of the main A and R peaks. (For interpretation of the references to color in this figure legend, the reader is referred to the web version of this article.)

$$W_R = \frac{A_R}{0.884A_A + A_R} \quad (1)$$

where W_R is the weight percentage of rutile, A_R the integrated area of (110) rutile peak (at 27.46°) and A_A the integrated area of (101) anatase peak (at 25.30°). The results are indicated in Table 1. Cell parameters a and c of the tetragonal anatase structure were calculated considering the position of the peaks at 2θ = 37.83° and 48.09° corresponding to the planes (004) and (200), respectively. The results obtained for CAD films differed in < 0.2% with respect to the values corresponding to bulk anatase (a = 3.7852 Å and c = 9.5139 Å; ICDD reference card 00-021-1272). Anatase crystallite size was determined using Scherrer's equation from the broadening of the main A peak. The crystallite size tended to increase with the film thickness; the values found were ~100 nm for CAD 200 and CAD 400, ~110 nm for CAD 750 and CAD 900, and ~150 nm for CAD 1000 and CAD 1100. According to the previous work [15], the crystalline structure of powder P25 was maintained for films prepared by dip-coating.

SEM images obtained from the surface of CAD and P25 films are shown in Fig. 2. Fig. 2a exhibits a typical surface morphology of P25 films in a picture corresponding to the sample P25 100. Fig. 2b, c and d show the surface of samples CAD 200, CAD 750 and CAD 1100, respectively. It can be seen that the P25 film was clearly more porous than CAD films. On the other hand, CAD films exhibited some fissures, which were more noticeable in the thickest films. The surface of CAD films was composed of grains which were larger as the film was thicker. The presence of macroparticles, a typical feature in films deposited by unfiltered cathodic arc, was more noticeable for the thinnest films. The surface of CAD 400 was similar to that of CAD 200; while CAD 900 and CAD 1000 looked alike to CAD 750.

Fig. 3 shows transmittance spectra in the UV–visible range obtained from TiO_2 samples grown by CAD with different thickness. All the plots showed interference effects above 350 nm, which indicates a rather low roughness [44]. In the region of weak absorption (above 600 nm), all the films exhibited a mean transmittance in the range 60–70%; dependence of the mean transmittance on the film thickness was not noticeable. The shape of interference effects for the thinnest films indicates a uniform thickness. The evidenced beat signals would indicate that the density was not quite uniform in the thickest samples. From the wavelength corresponding to interference maxima and minima, and using the thickness values presented in Table 1, the index of refraction of the films were estimated [44]. All values lied in the range 2.6 ± 0.6.

Fig. 4 shows the UV–Vis transmittance spectra of the P25 films obtained by dip-coating. The absence of interference effects indicates a higher roughness for P25 films compared to CAD samples. A clear dependence of the transmittance with the thickness of the TiO_2 film could be observed, with the transmittance decreasing as the thickness increases at all wavelengths. In contrast with the films obtained by CAD, the P25 films were light dispersive, i.e., the film transmittance is a combination of both absorption and dispersion. Additionally, for the P25 480 sample, the transmittance at wavelengths below 400 nm was almost negligible; thus, it can be inferred that a thicker film would not increase significantly the amount of light that could be used in the photocatalytic reaction. Even for the thinnest film, the P25 100 sample, the transmittance at $\lambda \leq 400$ nm was smaller than 35%, indicating that most of the photocatalytically active irradiation was either absorbed or dispersed.

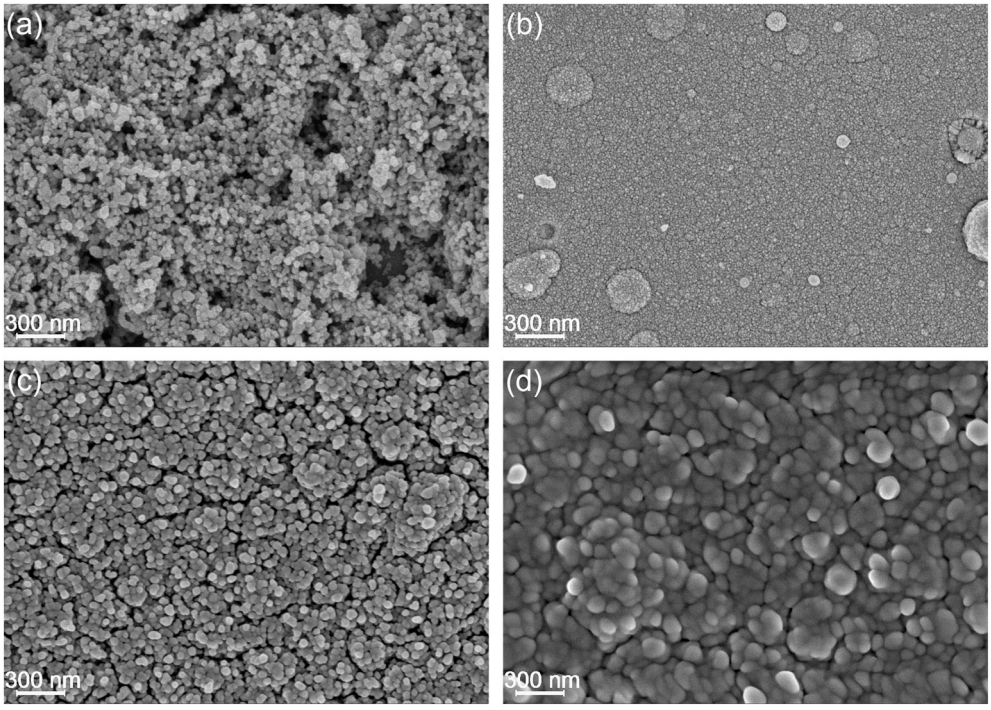

Fig. 2. SEM images obtained from the surface of (a) P25 100, (b) CAD 200, (c) CAD 750 and (d) CAD 1100.

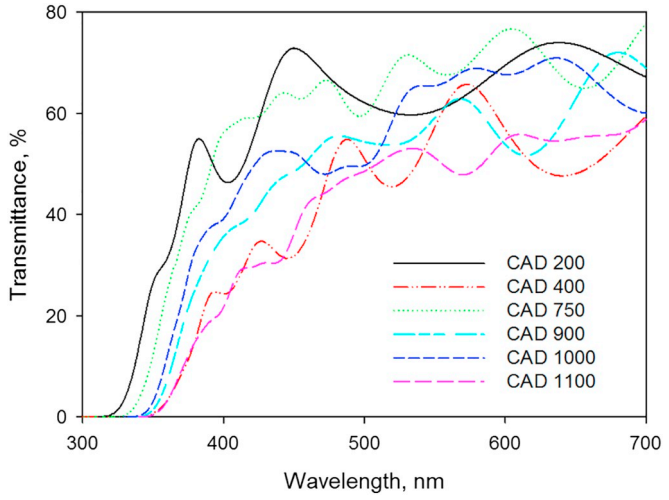

Fig. 3. Transmittance vs. wavelength plots for TiO_2 films grown by CAD with different thickness.

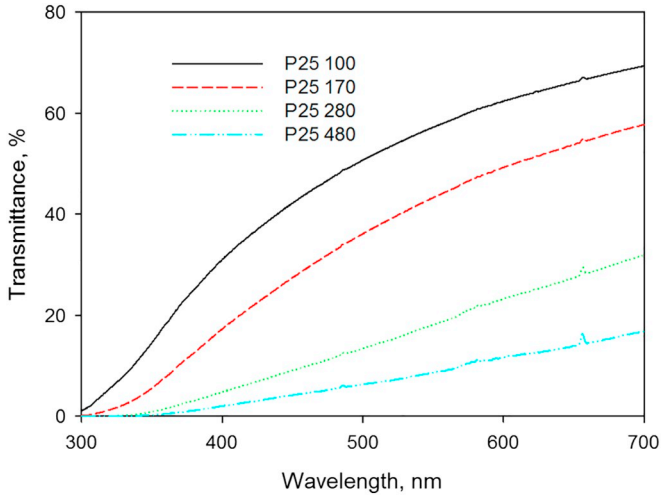

Fig. 4. Transmittance vs. wavelength plots for TiO_2 films prepared by dip-coating of glass substrates in P25 TiO_2 suspensions with different thickness.

3.2. Effect of the film thickness on the photocatalytic activity

Results obtained from photocatalytic tests performed over CAD and P25 films with the lowest (CAD 200 and P25 100) and highest (CAD 1100 and P25 480) thickness are depicted in Fig. 5, where the evolution of normalized Cr(VI) concentration ($[Cr(VI)]/[Cr(VI)]_0$) is plotted. Results of experiments with P25 suspensions at the same TiO_2 concentration as that used in the experiments with the P25 100 film (SP25 1) and with the standard 1 g L^{-1}concentration (SP25 3), and for the system in the absence of photocatalyst film (blank) are also shown. Cr (VI) concentration after 300 min irradiation for all the samples is reported in Table 2. In the blank experiment, a reduction of 53% of the initial Cr(VI) could be observed after 300 min, due to the homogeneous photochemical reduction of Cr(VI) under UV-A irradiation when alcohols and carboxylic acids are present (see [15] and references therein). It can be seen that all the films enhanced the Cr(VI) reduction in comparison with the blank in the absence of TiO_2. Besides, the photocatalytic activity increased with the film thickness for both types of films, although the suspended TiO_2 was much more efficient. The comparison of CAD and P25 films with the lowest thickness reveals that the latter exhibited a better photocatalytic performance, probably due to the higher porosity of the P25 films, as reported previously [15]. However, for the thickest films the photocatalytic activity was higher for the CAD film, Cr(VI) being fully reduced after 4 h irradiation; in contrast for the P25 480 film Cr(VI) could be still detected at the end of the experiment (Table 2). In all cases, when a significant Cr(VI) reduction was observed (> 80% of initial Cr(VI)), the color of the solution turned from yellow to pink due to the formation of Cr(III)-EDTA (see photo of the solution before and after treatment with CAD 1100 in Fig. S2, in the Supplementary Material file), as previously observed with TiO_2 in suspension [4,27]. The presence of Cr(III)-EDTA can be observed in the absorbance spectra (Fig. 6) of the solutions

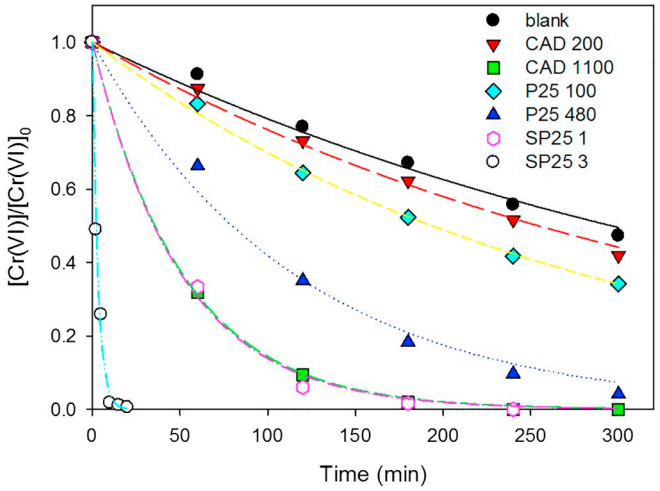

Fig. 5. Temporal evolution of normalized Cr(VI) concentration during photocatalytic tests over CAD and P25 films and P25 suspensions. Conditions: $[Cr(VI)]_0 = 0.8$ mM, $[EDTA]_0 = 1$ mM, pH 2 ($HClO_4$), $E = 2800\ \mu W\ cm^{-2}$. Lines: fittings to pseudo-first order kinetics (Eq. (2)).

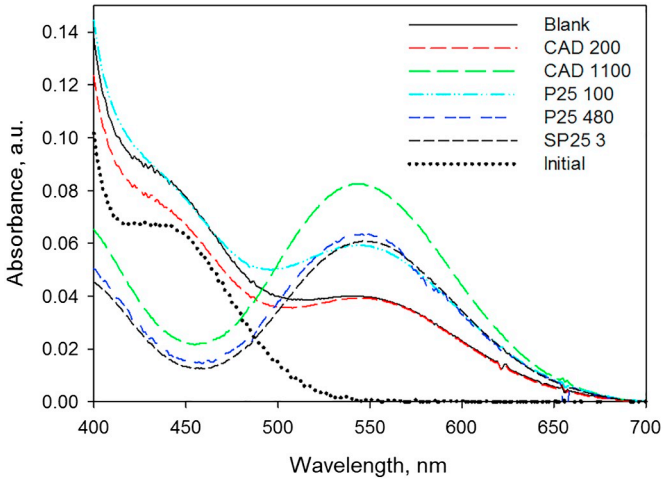

Fig. 6. Spectra of the solutions at the beginning (initial) and at the end of the experiments shown in Fig. 5. Conditions of Fig. 5. Suspended TiO_2 was removed from sample SP25 3 before measurement.

corresponding to final irradiation times of the experiments of Fig. 5 by the characteristic peak with a maximum at $\lambda = 540$ nm [4,27,37], which did not appear in the absorbance spectrum of the initial solution.

The Cr(III)-EDTA spectra was more clearly defined in the experiments where a complete or almost complete Cr(VI) reduction was obtained: CAD 1100, P25 480 and SP25 3; Cr(III)-EDTA concentrations at the end of the experiments are indicated in Table 2.

Experimental points of the runs with all the films were fitted to a pseudo-first order kinetics (Eqs. (2) and (3)), which includes a pseudo-first order kinetic constant k corresponding to the contribution of the homogeneous Cr(VI) photochemical reduction in the presence of EDTA, and a pseudo-first order kinetic constant k' that represents the contribution of the heterogeneous photocatalytic process. The value of k was calculated from blank experiments without TiO_2 ($k' = 0$) and set fixed in the experiments with TiO_2 to estimate the value of k'.

$$\frac{d[Cr(VI)]}{dt} = (k + k') \times [Cr(VI)] \tag{2}$$

$$\frac{[Cr(VI)]}{[Cr(VI)]_0} = e^{(k+k')\times t} \tag{3}$$

The values of k and k' are indicated in Table 2, together with the correlation coefficient (R^2), the final concentration of Cr(VI) and Cr (III)-EDTA remaining in solution after 300 min of irradiation, and the percentage of the reduced Cr(VI) that is transformed into Cr(III)-EDTA in solution.

Results obtained in all cases were also fitted using the more complex zero + first order kinetics (the pseudo-first order constant is fixed according to the blank and the zero order constant is related to the film efficiency) proposed in previous works [11,15,16], and R^2 values for fittings with the two proposed kinetics were compared (see Fig. S3, in the Supplementary Material file). For films with relatively lower activity the R^2 values obtained by fitting with zero + first order kinetics were almost identical to those obtained with the simpler pseudo-first order kinetics, while this latter kinetics fitted much better the results obtained with the most active films, as also observed by Vera et al. [16]. Therefore, the pseudo-first order kinetics gives an adequate fitting of the experimental results for all the samples studied in this work. This fact indicates that the Cr(VI) concentration in solution is at least one of the controlling parameters, especially for the films with higher photocatalytic activity.

For both CAD and P25 samples, the values of k' shown in Table 2 increased as the film thickness increased; the best samples (CAD 1000 and CAD 1100) led to complete Cr(VI) reduction after 300 min of irradiation. As usually observed in photocatalytic systems, for a given TiO_2 concentration in solution, the photocatalytic rate was always lower for films compared with the suspensions [3,15,45] due to mass and light transport limitations and to sintering among particles; both phenomena decreases specific surface and may enhance electron-hole

Table 2
TiO_2 concentration, pseudo-first order kinetic constants, correlation coefficients (R^2), Cr(VI) and Cr(III)-EDTA concentrations and Cr(III)-EDTA yield after 300 min of UV–Vis irradiation for the experiments of Fig. 5.

Sample	$[TiO_2]$ (mg L^{-1})	$k' \times 10^3$ (min^{-1})	R^2	[Cr(VI)] at 300 min (mM)	[Cr(III)-EDTA] at 300 min (mM)	Cr(III)-EDTA yield (%)
CAD 200	50 ± 10	0.39 ± 0.07	0.994	0.34	0.28	61
CAD 400	100 ± 10	1.3 ± 0.1	0.995	0.25	0.35	64
CAD 750	180 ± 20	11 ± 1	0.99	0.01	0.57	72
CAD 900	210 ± 20	9.1 ± 0.2	0.999	0.02	0.62	79
CAD 1000	250 ± 20	16 ± 1	0.996	0.00	0.60	75
CAD 1100	280 ± 20	16.9 ± 0.2	1	0.00	0.59	74
P25 100	19 ± 1	1.3 ± 0.1	0.998	0.25	0.40	73
P25 170	30 ± 2	2.4 ± 0.1	0.996	0.19	0.37	61
P25 280	50 ± 3	5.6 ± 0.4	0.987	0.07	0.43	59
P25 480	87 ± 5	6.9 ± 0.6	0.989	0.03	0.45	58
SP25 1	20 ± 1	18 ± 1	0.997	0.00	–	–
SP25 2	90 ± 2	56 ± 4	0.994	0.00	–	–
SP25 3	1000 ± 10	310 ± 20	0.993	0.00	0.43	54
Blank	–	2.4 ± 0.1[a]	0.98	0.38	0.34	81

[a] Corresponding to the pseudo-first order kinetic constant k.

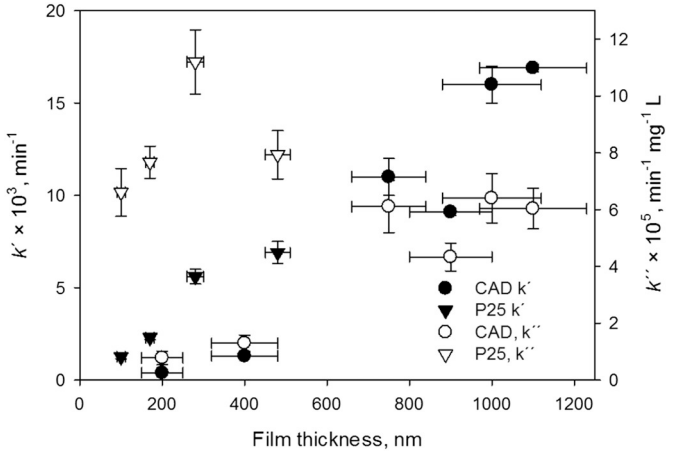

Fig. 7. Pseudo-first order rate constant of the photocatalytic reaction ($k´$) and TiO_2-mass normalized pseudo-first order rate constant ($k´´$) as a function of thickness for both types of films. Conditions of Fig. 5.

recombination. The yield of Cr(III)-EDTA did not show a clear behavior, with values between 58 and 79%, indicating that most of the formed Cr (III) remained soluble as Cr(III)-EDTA complexes. For SP25 3, the yield was similar to that obtained with the thickest P25 films (P25 280 and P25 480); this indicates that, for a given material, the TiO_2 concentration may be a more important factor on the product distribution of Cr(VI) reduction (i.e., Cr(III) free or complexed in solution, or deposited over the TiO_2 surface) than if TiO_2 is suspended or immobilized.

Fig. 7 shows the values of $k´$ and mass normalized rate constant ($k´´$), defined as the pseudo-first order photocatalytic rate constant divided by the TiO_2 mass of the film. Considering films with the same thickness, Fig. 7 shows clearly that P25 samples were more efficient photocatalysts; however, while the thickness of P25 films cannot be increased, CAD samples can be tailored to get a higher thickness and thus reach a higher photocatalytic performance. Increasing the activity by increasing the thickness has been observed in photocatalytic experiments over titania films prepared by different techniques [11,15–17,23–25,46]. Depending on the diffusivity of the reagents and the fraction of light absorbed, an optimal film thickness can be reached, beyond which the photocatalytic activity is no longer significantly enhanced, or it even decreases in some cases, for instance, when the samples are illuminated from the back side through a transparent substrate [23–25,47,48]. Optimal thicknesses have been reported for 10 μm [46] and 25 μm [49] for degradation of 4-chlorobenzoic acid and methylene blue, respectively, using TiO_2 films prepared by sol-gel. The density of the films is somewhat smaller than that corresponding to bulk A (3.89 g cm^{-3} [50]) indicating that the films (especially those of P25) are porous; thus, the increase in the photocatalytic degradation rate with the increasing thickness of the films can be also related to the increase in the total surface. It is important to point out that the most active films (CAD 1000 and CAD 1100) were composed of minor amounts of rutile, which could also contribute to the higher photocatalytic activity of these films because the migration of photogenerated electrons in rutile to the conduction band of anatase can lead to a decrease of electron-hole recombination ([11] and references therein). However, the results here obtained do not allow to indicate to what extent the rutile phase contributes to the Cr(VI) photocatalytic reduction.

When comparing with other pseudo-first order kinetic constants reported for Cr(VI) photocatalytic reduction with immobilized TiO_2 (see Table in section S4, Supplementary Material file), it can be observed that the value of $k´$ for CAD 1100 (the most active film) is in the same order of magnitude, although most experiments were performed with an initial Cr(VI) concentration up to 40 times lower. This clearly reinforces the conclusion that the reaction rate for CAD 1100 is much higher.

The value of $k´´$ increased for the CAD samples when the thickness increased from 200 to 750 nm, where it reached an almost constant value (Fig. 7). In contrast, for the P25 samples, an increase could be observed when the thickness increased from 100 to 280 nm, followed by a decrease for the 480 nm sample, indicating that an optimal value was reached. This increase in $k´´$ with the increase of the film thickness can be related to the deactivation of TiO_2 caused by deposition of Cr (III), as largely reported in the literature [4,27,28,41,51–53], which should be more pronounced for the samples with lower TiO_2 mass, as this deactivation is proportional to the ratio between the concentration of Cr(III) deposited and the TiO_2 concentration ($[Cr(III)_{dep}]/[TiO_2]$).

Meichtry et al. have found no deactivation during the photocatalytic reduction of Cr(VI) in the presence of EDTA when using P25 in suspension (1 g L^{-1}) [27]. However, the conditions in the present case are different, as the photocatalyst was immobilized and lower concentrations of TiO_2 (≤ 0.28 g L^{-1}) and EDTA were used.

3.3. Reuse of the films

The three thickest CAD films (CAD 900, CAD 1000 and CAD 1100), together with the P25 100 film, were studied for their reuse in the photocatalytic Cr(VI) reduction under the same conditions as those indicated in the previous section; the experiments were numbered, with n representing the n^{th} use of the sample. The results obtained with $1 \leq n \leq 4$ are presented in Table 3 and in Fig. 8 where the pseudo-first order rate constant $k´_n$, normalized with respect to the $k´_1$ value indicated in Table 3 ($k´_n / k´_1$), vs. n is plotted.

For all the studied films, the photocatalytic activity diminished after the successive uses until the value of $k´_n / k´_1$ for the fourth experiment was approximately 1/3 of the initial value for the three CAD films. For the P25 100 film, a decrease (55% smaller than the initial value) could be observed only at the third experiment, remaining almost constant during the fourth experiment. This decrease in $k´$ after four experiments is similar to that reported for Cr(VI) reduction with supported P25 TiO_2 films using tartaric ($k´_4 / k´_1 = 0.61$ [23]) or citric acids ($k´_4 / k´_1 = 0.56$ [24]) as donors, despite the authors used far lower $[Cr(VI)]_0/[TiO_2]$ ratios and thus, lower $[Cr(III)_{dep}]/[TiO_2]$ should be expected in those works. Correspondingly, the deactivation should be more pronounced for the samples tested in this work; therefore, the

Table 3
Pseudo-first order kinetic constant $k´$, correlation coefficient (R^2), Cr(VI) and Cr (III)-EDTA concentrations, and Cr(III)-EDTA yield after 300 min of UV–Vis irradiation for the experiments performed with the different TiO_2 films and suspensions. Conditions: $[Cr(VI)]_0 = 0.8$ mM, $[EDTA]_0 = 1$ mM, pH 2 ($HClO_4$), $E = 2800$ μW cm^{-2}.

Sample	n	$k´ \times 10^3$ (min^{-1})	R^2	[Cr(VI)] at 300 min (mM)	[Cr(III)-EDTA] at 300 min (mM)	Cr(III)-EDTA yield (%)
CAD 900	1	9.1 ± 0.2	0.999	0.02	0.62	79
	2	4.3 ± 0.2	0.993	0.08	0.53	75
	3	4.3 ± 0.2	0.995	0.08	0.49	68
	4	2.6 ± 0.2	0.992	0.13	0.50	75
CAD 1000	1	16 ± 1	0.996	0.00	0.60	75
	2	8.0 ± 0.7	0.983	0.00	0.64	80
	3	6.7 ± 0.7	0.982	0.00	0.60	75
	4	4.5 ± 0.5	0.983	0.04	0.63	83
CAD 1100	1	16.9 ± 0.2	1	0.00	0.59	74
	2	11 ± 1	0.990	0.00	0.69	86
	3	11 ± 1	0.978	0.00	0.53	66
	4	5.4 ± 0.6	0.984	0.02	0.60	77
P25 100	1	1.3 ± 0.1	0.998	0.25	0.40	73
	2	1.3 ± 0.1	0.998	0.27	0.42	79
	3	0.58 ± 0.07	0.996	0.30	0.44	88
	4	0.62 ± 0.02	0.996	0.24	0.52	93

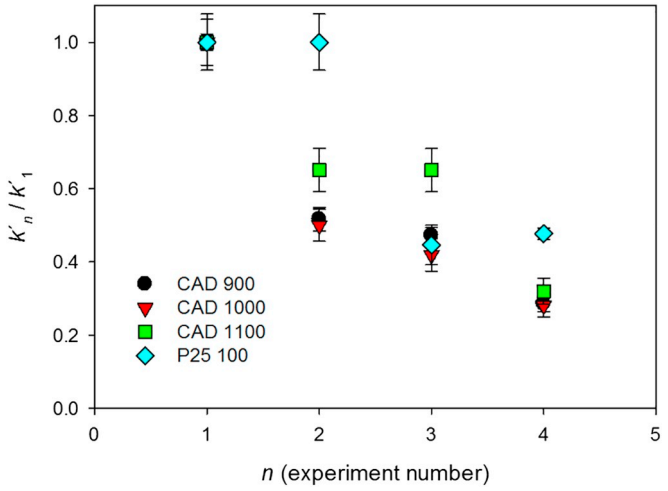

Fig. 8. Normalized rate constant of the photocatalytic reaction for successive uses of both types of films. Conditions of Fig. 5.

similar decrease in k'_4 / k'_1 can be ascribed to the protective effect of EDTA compared to other carboxylic acids [27,28].

As during this fourth experiment with the P25 100 film almost all reduced Cr(VI) remained in solution as Cr(III)-EDTA (see Table 3), Cr (III) deposition and the consequent TiO_2 deactivation [4,27,28,41] no longer takes place; therefore, k'_4 can be considered the final value of this parameter. For the CAD films, no clear tendency was observed in the Cr(III)-EDTA yield, but the yield values ($\leq$86%) and the continuous decrease in k'_n clearly indicates that Cr(III) deposition and TiO_2 deactivation are taking place. From a practical point of view, this deactivation does not mean that the films should be replaced after a given time, as Cr(III) can be removed from the TiO_2 surface using a citric acid or EDTA solution [54], thus regenerating the photocatalyst. It should be emphasized that despite the decrease of the photocatalytic activity was more significant for the CAD films, at $n = 4$ the value of k' for the CAD 1100 film was one order of magnitude higher than the one obtained for P25 100, and an almost complete Cr(VI) removal was obtained after 300 min, indicating that the photocatalytic activity was still much higher for the CAD 1100 film.

4. Conclusions

TiO_2 films obtained by cathodic arc deposition showed a high photocatalytic activity toward Cr(VI) reduction compared with P25 TiO_2 films. The photocatalytic reaction for Cr(VI) reduction in the presence of EDTA was used as an excellent system to test the photocatalytic efficiency of the films. A pseudo-first order kinetics was found to be followed by all the studied TiO_2 samples. The photocatalytic efficiency increased as the thickness increased, P25 films showing higher photoactivity in the Cr(VI)/EDTA system than CAD films of similar thickness. However, the possibility of increasing the thickness allows CAD samples to achieve a higher efficiency than P25 films, attaining a full reduction of Cr(VI) after 4 h. As the optimal thickness mentioned in the literature was not reached along the studied thickness range, thus, the performance of CAD films could be further enhanced. After reuse, the films showed a decrease in the rate constant of the reaction for both P25 and CAD films related to the deactivation caused by Cr(III) deposition, this decline being more marked for the CAD films. Despite this, most active CAD films remain more active than P25 samples.

Author contribution

A. Kleiman: Conceptualization, Methodology, Formal Analysis, Investigation, Writing- Original draft, Writing- Reviewing and Editing. J.M. Meichtry: Conceptualization, Methodology, Formal Analysis, Investigation, Writing- Original draft, Writing- Reviewing and Editing. D. Vega: Investigation, Writing- Reviewing and Editing. M.I. Litter: Conceptualization, Methodology, Writing- Reviewing and Editing, Supervision, Funding acquisition. A. Márquez: Conceptualization, Methodology, Writing- Reviewing and Editing, Supervision, Funding acquisition.

Declaration of competing interest

The authors declare that they have no known competing financial interests or personal relationships that could have appeared to influence the work reported in this paper.

Acknowledgments

This work was supported by grants from University of Buenos Aires (PID 20020150100103BA), CONICET (PIP 11220170100711CO), Agencia Nacional de Promoción Científica y Tecnológica (ANPCyT) from Argentina (PICT-2011-0463, PICT-2015-0208 and PICT 2015-2285) and BioCritical Metals (ERAMIN 2015 grant). Transmittance measurements in CAD films were performed at Laboratorio de Polímeros y Materiales Compuestos (LP&MC), Physics Department, FCEyN, University of Buenos Aires. The authors would like to thank Diego Lamas and Ana Larralde for XRD measurements performed at Laboratorio de Cristalografía Aplicada, Universidad Nacional de General San Martín.

Appendix A. Supplementary data

Supplementary data to this article can be found online at https://doi.org/10.1016/j.surfcoat.2019.125154.

References

[1] K. Nakata, A. Fujishima, TiO_2 photocatalysis: design and applications, J. Photochem. Photobiol. C 13 (2012) 169–189, https://doi.org/10.1016/j.jphotochemrev.2012.06.001.
[2] H. Gerischer, Solar photoelectrolysis with semiconductor electrodes, in: B.O. Seraphin (Ed.), Solar Energy Conversion, Topics in Applied Physics, vol 31, Springer, Berlin, Heidelberg, 1979, pp. 115–172.
[3] S.K. Loeb, P.J.J. Alvarez, J.A. Brame, E.L. Cates, W. Choi, J. Crittenden, D. D. Dionysiou, Q. Li, G. Li-Puma, X. Quan, D.L. Sedlak, T.D. Waite, P. Westerhoff, J.-H. Kim, The technology horizon for photocatalytic water treatment: sunrise or sunset?, Environ. Sci. Technol. 53 (2019) 2937–294. doi:https://doi.org/10.1021/acs.est.8b05041.
[4] J.M. Meichtry, C. Colbeau-Justin, G. Custo, M.I. Litter, TiO_2-photocatalytic transformation of Cr(VI) in the presence of EDTA: comparison of different commercial photocatalysts and studies by time resolved microwave conductivity, Appl. Catal. B Environ. 144 (2014) 189–195, https://doi.org/10.1016/j.apcatb.2013.06.032.
[5] D.C. Hurum, A.G. Agrios, K.A. Gray, T. Rajh, M.C. Thurnauer, Explaining the enhanced Photocatalytic activity of degussa P25 mixed-phase TiO_2 using EPR, J. Phys. Chem. B 107 (2003) 4545–4549, https://doi.org/10.1021/jp0273934.
[6] L. Zhang, R. Dillert, D. Bahnemann, M. Vormoor, Photo-induced hydrophilicity and self-cleaning: models and reality, Energy & Environ. Sci. 5 (2012) 7491–7507, https://doi.org/10.1039/C2EE03390A.
[7] J. Schneider, M. Matsuoka, M. Takeuchi, J. Zhang, Y. Horiuchi, M. Anpo, D.W. Bahnemann, Understanding TiO_2 photocatalysis: mechanisms and materials, Chem. Rev. 114 (2014) 9919–9986, https://doi.org/10.1021/cr5001892.
[8] J. Ananpattarachai, P. Paksaharn, P. Kajitvichyanukul, Photocatalytic reduction of chromium (VI) in aqueous solutions by nano-TiO_2 thin film in rotating disc photoreactor, Int. J. Environ. Waste Manag. 17 (2016) 176–188, https://doi.org/10.1504/IJEWM.2016.076754.
[9] Y. Zhao, W. Chang, Z. Huang, X. Feng, L. Ma, X. Qi, Z. Li, Enhanced removal of toxic Cr(VI) in tannery wastewater by photoelectrocatalysis with synthetic TiO_2 hollow spheres, Appl. Surf. Sci. 405 (2017) 102–110, https://doi.org/10.1016/j.apsusc.2017.01.306.
[10] P. Sane, S. Chaudhari, P. Nemade, S. Sontakke, Photocatalytic reduction of chromium (VI) using combustion synthesized TiO_2, J. Environ. Chem. Eng. 6 (2018) 68–73, https://doi.org/10.1016/j.jece.2017.11.060.
[11] H.D. Traid, M.L. Vera, A.E. Ares, M.I. Litter, Advances on the synthesis of porous TiO_2 coatings by anodic spark oxidation. Photocatalytic reduction of Cr(VI), Mater. Chem. Phys. 191 (2017) 106–113, https://doi.org/10.1016/j.matchemphys.2017.01.034.
[12] L. Ling, L. Liu, Y. Feng, J. Zhu, Z. Bian, Synthesis of TiO_2 mesocrystal film with

enhanced photocatalytic activity, Chinese J. Catal. 39 (2018) 639–645, https://doi.org/10.1016/S1872-2067(17)62980-2.
[13] M. Kazemi, M. Jahanshahi, M. Peyravi, Hexavalent chromium removal by multi-layer membrane assisted by photocatalytic couple nanoparticle from both permeate and retentate, J. Hazard. Mater. 344 (2018) 12–22, https://doi.org/10.1016/j.jhazmat.2017.09.059.
[14] M.I. Litter, Last advances on TiO2-photocatalytic removal of chromium, uranium and arsenic, Current Opinion in Green Sustain. Chem. 6 (2017) 150–158, https://doi.org/10.1016/j.cogsc.2017.04.002.
[15] A. Kleiman, A. Márquez, M.L. Vera, J.M. Meichtry, M.I. Litter, Photocatalytic activity of TiO_2 thin films deposited by cathodic arc, Appl. Catal. B Environ. 101 (2011) 676–681, https://doi.org/10.1016/j.apcatb.2010.11.009.
[16] M.L. Vera, H.D. Traid, E.R. Henrikson, A.E. Ares, M.I. Litter, Heterogeneous photocatalytic Cr(VI) reduction with short and long nanotubular TiO_2 coatings prepared by anodic oxidation, Mat. Res. Bull. 97 (2018) 150–157, https://doi.org/10.1016/j.materresbull.2017.08.013.
[17] P. Kajitvichyanukul, J. Ananpattarachai, S. Pongpom, Sol–gel preparation and properties study of TiO_2 thin film for photocatalytic reduction of chromium(VI) in photocatalysis process, Sci. Technol. Adv. Mater. 6 (2005) 352–358, https://doi.org/10.1016/j.stam.2005.02.014.
[18] D.M. Hausladen, A. Alexander-Ozinskas, C. McClain, S. Fendorf, Hexavalent chromium sources and distribution in California groundwater, Environ. Sci. Technol. 52 (2018) 8242–8251, https://doi.org/10.1021/acs.est.7b06627.
[19] M.I. Litter, N. Quici, J.M. Meichtry, A.M. Senn, Photocatalytic removal of metallic and other inorganic pollutants, in: D.D. Dionysiou, G. Li Puma, J. Ye, J. Schneider, D. Bahnemann (Eds.), Photocatalysis: Applications, Royal Society of Chemistry, Cambridge, 2016, pp. 35–71.
[20] M.I. Litter, N. Quici, J.M. Meichtry, V.N. Montesinos, Photocatalytic treatment of inorganic materials with TiO_2 nanoparticles, in: H.S. Nalwa (Ed.), Encyclopedia of Nanoscience and Nanotechnology, Vol. 29 American Scientific Publishers, Valencia, California, 2018, pp. 303–336.
[21] M.I. Litter, Mechanisms of removal of heavy metals and arsenic from water by TiO_2-heterogeneous photocatalysis, Pure Appl. Chem. 87 (6) (2015) 557–567, https://doi.org/10.1515/pac-2014-0710.
[22] S. Zheng, Z. Xu, Y. Wang, Z. Wei, B. Wang, On the enhanced catalytic activity of TiO_2-supported layered compounds for Cr(VI) photo-reduction, J. Photochem. Photobiol. A Chem. 137 (2000) 185–189, https://doi.org/10.1016/S1010-6030(00)00370-1.
[23] B.A. Marinho, R. Djellabi, R.O. Cristovão, J.M. Loureiro, R.A.R. Boaventura, M.M. Dias, J.C.B. Lopes, V.J.P. Vilar, Intensification of heterogeneous TiO_2 photocatalysis using an innovative micro–meso-structured-reactor for Cr(VI) reduction under simulated solar light, Chem. Eng. J. 318 (2017) 76–88, https://doi.org/10.1016/j.cej.2016.05.077.
[24] B.A. Marinho, R.O. Cristovão, R. Djellabi, J.M. Loureiro, R.A.R. Boaventura, V.J.P. Vilar, Photocatalytic reduction of Cr(VI) over TiO_2-coated cellulose acetate monolithic structures using solar light, App. Catal. B 203 (2017) 18–30, https://doi.org/10.1016/j.apcatb.2016.09.061.
[25] B.A. Marinho, R.O. Cristovão, R. Djellabi, A. Caseiro, S.M. Miranda, J.M. Loureiro, R.A.R. Boaventura, M.M. Dias, J.C.B. Lopes, V.J.P. Vilar, Strategies to reduce mass and photon s transfer limitations in heterogeneous photocatalytic processes: hexavalent chromium reduction studies, J. Environ. Manag. 217 (2018) 555–564, https://doi.org/10.1016/j.jenvman.2018.04.003.
[26] J. Sabate, M.A. Anderson, M.A. Aguado, J. Giménez, S. Cervera-March, C.G. Hilld Jr., Comparison of TiO_2 powder suspensions and TiO_2 ceramic membranes supported on glass as photocatalytic systems in the reduction of chromium(VI), J. Molec. Catal. 71 (1992) 57–68, https://doi.org/10.1016/0304-5102(92)80007-4.
[27] J.M. Meichtry, C. Colbeau-Justin, G. Custo, M.I. Litter, Preservation of the photocatalytic activity of TiO_2 by EDTA in the reductive transformation of Cr(VI). Studies by time resolved microwave conductivity, Catal. Today 224 (2014) 236–243, https://doi.org/10.1016/j.cattod.2013.10.021.
[28] V.N. Montesinos, C. Salou, J.M. Meichtry, C. Colbeau-Justin, M.I. Litter, Role of Cr (III) deposition during the photocatalytic transformation of hexavalent chromium and citric acid over P25 and UV100, Photochem. Photobiol. Sci. 15 (2016) 228–234, https://doi.org/10.1039/C5PP00420A.
[29] A. Bendavid, P.J. Martin, E.W. Preston, The effect of pulsed direct current substrate bias on the properties of titanium dioxide thin films deposited by filtered cathodic vacuum arc deposition, Thin Solid Films 517 (2008) 494–499, https://doi.org/10.1016/j.tsf.2008.06.060.
[30] A. Bendavid, P.J. Martin, Review of thin film materials deposition by the filtered cathodic vacuum arc process at CSIRO, J. Australian Ceram. Soc. 50 (2014) 86–101 https://www.researchgate.net/publication/261762263_Review_of_thin_film_materials_deposition_by_the_filtered_cathodic_vacuum_arc_process_at_CSIRO.
[31] V. Jokanović, B. Čolović, A. Trajkovska Petroska, A. Mraković, B. Jokanović, M. Nenadović, M. Ferrara, I. Nasov, Optical properties of titanium oxide films obtained by cathodic arc plasma deposition, Plasma Sci. Technol. 19 (2017), https://doi.org/10.1088/2058-6272/aa8806.
[32] M. Lilja, J. Forsgren, K. Welch, M. Åstrand, H. Engqvist, M. Strømme, Photocatalytic and antimicrobial properties of surgical implant coatings of titanium dioxide deposited though cathodic arc evaporation, Biotechnol. Lett. 34 (2012) 2299–2305, https://doi.org/10.1007/s10529-012-1040-2.
[33] B. Kepenek, S. Öncel, A.F. Çakir, M. Ürgen, Photoactive TiO_2 coatings on metal substrates by cathodic arc deposition technique, Key Eng. Mater. 264–268 (2004) 549–552, https://doi.org/10.4028/www.scientific.net/KEM.264-268.549.
[34] B. Kepenek, U. Seker, A.F. Cakir, M. Ürgen, C. Tamerler, Photocatalytic bactericidal effect of TiO_2 thin films produced by cathodic arc deposition method, Key Eng. Mat. 254–256 (2004) 463–466, https://doi.org/10.4028/www.scientific.net/KEM.254-256.463.
[35] A. Márquez, G. Blanco, M.E. Fernandez de Rapp, D.G. Lamas, R. Tarulla, Properties of cupric oxide coatings prepared by cathodic arc deposition, Surf. Coat. Technol. 187 (2004) 154–160, https://doi.org/10.1016/j.surfcoat.2004.02.009.
[36] ASTM Standards D 1687-92, (1999).
[37] Z. Marczenko, M. Balcerzak, Separation, Preconcentration, and Spectrophotometry in Inorganic Analysis, Analytical Spectroscopy Library, Elsevier, Amsterdam, 2000.
[38] A.D. Bokare, W. Choi, Advanced oxidation process based on the Cr(III)/Cr(VI) redox cycle, Environ. Sci. Technol. 45 (2011) 9332–9338, https://doi.org/10.1021/es2021704.
[39] G.J. Puzon, A.G. Roberts, D.M. Kramer, L. Xun, Formation of soluble organo−-chromium(III) complexes after chromate reduction in the presence of cellular organics, Environ. Sci. Technol. 39 (2005) 2811–2817, https://doi.org/10.1021/es048967g.
[40] K.A. Easom, R.N. Bose, Reactions of aminopolycarboxylic acids with high-valent transition-metal ions: EDTA-assisted decomposition of carboxylato-bound chromium(V) complexes, Inorg. Chem. 27 (1988) 2331–2334, https://doi.org/10.1021/ic00286a022.
[41] N. Wang, Y. Xu, L. Zhu, X. Shen, H. Tang, Reconsideration to the deactivation of TiO_2 catalyst during simultaneous photocatalytic reduction of Cr(VI) and oxidation of salicylic acid, J. Photochem. Photobiol. A 201 (2009) 121–127, https://doi.org/10.1016/j.jphotochem.2008.10.002.
[42] A. Kleiman, D.G. Lamas, A.F. Craievich, A. Márquez, X-ray reflectivity analysis of titanium dioxide thin films grown by cathodic arc deposition, J. Nanosci. Nanotechnol. 14 (2014) 3902–3909, https://doi.org/10.1166/jnn.2014.8017.
[43] A.A. Gribb, J.F. Banfield, Particle size effects on transformation kinetics and phase stability in nanocrystalline TiO_2, Am. Mineral. 82 (1997) 717–728, https://doi.org/10.2138/am-1997-7-809.
[44] R. Swanepoel, Determination of the thickness and optical constants of amorphous silicon, J. Phys. E: Sci. Instrum. 16 (1983) 1214–1222, https://doi.org/10.1088/0022-3735/16/12/023.
[45] G. Piperata, J.M. Meichtry, M.I. Litter, Photocatalytic reactions over TiO_2 supported on porcelain spheres, Progr. Colloid Polym. Sci. 128 (2004) 303–308, https://doi.org/10.1007/b97123.
[46] Y. Chen, D.D. Dionysiou, Correlation of structural properties and film thickness to photocatalytic activity of thick TiO_2 films coated on stainless steel, Appl. Catal. B Environ. 69 (2006) 24–33, https://doi.org/10.1016/j.apcatb.2006.05.002.
[47] G. Camera-Roda, F. Santarelli, Optimization of the thickness of a photocatalytic film on the basis of the effectiveness factor, Catal. Today 129 (2007) 161–168, https://doi.org/10.1016/j.cattod.2007.06.062.
[48] A. Mills, S.-K. Lee, A. Lepre, I.P. Parkin, S.A. O'Neill, Spectral and photocatalytic characteristics of TiO_2 CVD films on quartz, Photochem. Photobiol. Sci. 1 (2002) 865–868, https://doi.org/10.1039/B205715H.
[49] H.K. Hakki, S. Allahyari, N. Rahemi, M. Tasbihi, The role of thermal annealing in controlling morphology, crystal structure and adherence of dip coated TiO_2 film on glass and its photocatalytic activity, Mater. Sci. Semicond. Process. 85 (2018) 24–32, https://doi.org/10.1016/j.mssp.2018.05.031.
[50] L. Wu, D. Buchholz, D. Bresser, L. Gomes Chagas, S. Passerini, Anatase TiO_2 nanoparticles for high power sodium-ion anodes, J. Power Sources 251 (2014) 379–385, https://doi.org/10.1016/j.jpowsour.2013.11.083.
[51] Y. Ku, I.-L. Jung, Photocatalytic reduction of Cr(VI) in aqueous solutions by UV irradiation with the presence of titanium dioxide, Water Res. 35 (2001) 135–142, https://doi.org/10.1016/S0043-1354(00)00098-1.
[52] H. Kyung, J. Lee, W. Choi, Simultaneous and synergistic conversion of dyes and heavy metal ions in aqueous TiO_2 suspensions under visible-light illumination, Environ. Sci. Technol. 39 (2005) 2376–2382, https://doi.org/10.1021/es0492788.
[53] H. Abdullah, D.-H. Kuo, Y.-H. Chen, High-efficient n-type TiO_2/p-type Cu_2O nanodiode photocatalyst to detoxify hexavalent chromium under visible light irradiation, J. Mater. Sci. 51 (2016) 8209–8223, https://doi.org/10.1007/s10853-016-0096-0.
[54] R. Djellabi, F.M. Ghorab, S. Nouacer, A. Smara, O. Khireddine, Cr(VI) photocatalytic reduction under sunlight followed by Cr(III) extraction from TiO_2 surface, Mat. Letters 176 (2016) 106–109, https://doi.org/10.1016/j.matlet.2016.04.090.